Journal of Applied Fluid Mechanics, Vol. 16, No. 5, pp. 1005-1016, 2023.
Available online at www.jafmonline.net, ISSN 1735-3572, EISSN 1735-3645.
https://doi.org/10.47176/jafm.16.05.1646

Numerical Analysis on the Unsteady Radial Load on the Shaft of a Large-Scale Dredge Pump Unit

L. Cao[1], T. Wu[1], T. Guo[1,2†], J. Hu[1] and J. Cao[3]

[1] *CCCC National Engineering Research Center of Dredging Technology and Equipment Co., Ltd., Shanghai, 200082, China*
[2] *School of Naval Architecture, Ocean and Civil Engineering, Shanghai Jiao Tong University, Shanghai, 200240, China*
[3] *State Key Laboratory of Hydroscience and Engineering & Department of Energy and Power Engineering, Tsinghua University, Beijing, 100084, China*

†*Corresponding Author Email: guotao@cccc-drc.com*

(Received November 2, 2022; accepted January 14, 2023)

ABSTRACT

Vibration and fatigue damage of pump shafts has become a prominent engineering problem, indicating the need for higher-quality reliability analysis of the pump unit in the design stage. In this study, the unsteady flow field in a large centrifugal dredge pump was numerically simulated via the unsteady Reynolds-averaged Navier-Stokes (URANS) method with the SST *k-ω* model. An experiment was carried out to verify the numerical method. The hydraulic radial force on the impeller and the total radial load were calculated based on computational fluid dynamics. The flow field with a double volute was simulated, analyzed, and compared to the flow field with a single volute. The stress of the pump shaft caused by the radial load was also calculated and discussed. The results show that the impeller gravity determines the time-averaged value and fluctuation frequency of the total radial load on the shaft, which must be considered in the shaft stability analysis. The total radial load fluctuating in asymmetric cycle results in stress cycles with different features at different circumferential locations. The application of a double volute effectively reduces the radial load on the pump shaft, which decreases the time-averaged hydraulic radial force by 38% and its fluctuation amplitude by 3%, decreases the time-averaged total radial load by 20% and its fluctuation amplitude by 28% in the design condition, and decreases the local stress at the narrowest shaft section by 44%. A double volute can be applied to weaken vibration and fatigue damage for a pump shaft if it is acceptable for the pump efficiency to be lowered.

Keywords: Centrifugal dredge pump; Radial force; Gravity; Shaft; Dynamic stress; Double volute.

NOMENCLATURE

A	amplitude	$\boldsymbol{u}$	flow velocity
Cp	pressure coefficient	u_2	circumferential velocity at the outlet of impelle
d	minimum shaft diameter	ρ	density of water
D_1	diameter of the suction pipe	σ	stress
D_2	outside diameter of the impeller	μ	dynamic viscosity
f	frequency	k	turbulence kinetic energy
f_n	rotational frequency	ω	turbulent frequency
$\boldsymbol{Fr}$	total radial load	μ_t	eddy viscosity
$\boldsymbol{Fr}_h$	hydraulic radial force	σ_k	constant in *k*-equation
Fx	X component of the radial force	σ_ω	constant in *ω*-equation
Fy	Y component of the radial force	β*	constant in *k*-equation
G_{imp}	weight of impeller	β	constant in *ω*-equation
H_d	design head	P_k	production rate of turbulence
n	rotational speed	F_1	a blending function in SST *k-ω* model
p_{atm}	atmospheric pressure	f_r	an empirical function of curvature correction
Q_d	design flow rate		

Abbreviations

CFD	Computational Fluid Dynamics
URANS	Unsteady Reynolds-Averaged Navier–Stokes
SST	Shear Stress Transport

Subscripts

ave	average value
d	design
h	hydraulic
m	peak value
max	maximum value
min	minimum value

1. INTRODUCTION

The dredge pump is a key piece of equipment in a dredger. Whether the pump unit runs efficiently, stably, and safely matters to the prospective value of the project it serves. The internal flow, which is non-uniform in space and unsteady in time, plays a decisive role in the pump performance, so it has received much attention in academia (Brennen 2011). In recent years, the increasing demand for large-scale dredge pumps alongside the development of large-scale construction engineering have presented greater challenges to the reliability of the pump unit. Taking the tailing suction hopper dredger as an example, the capacity of a tailing suction hopper dredger was typically below 3,000 m^3 before 2000, but since the turn of the 21st century, it has gradually increased to 10,000 m^3. Accordingly, the dimensions of the dredge pump have also increased gradually. Therefore, the pump shaft is more prone to vibration, fatigue damage, and mechanical seal failure during operation.

Dredge pumps are usually centrifugal pumps. There are two main causes of rotor vibration and shaft fatigue in centrifugal pump units: 1) the eccentric mass of a rotor due to poor machining quality or uneven wear leads to rotor imbalance during operations (Tan *et al.* 2021; Lu *et al.* 2022), and 2) the fluid excitation force exerted on the impeller has obvious unsteady characteristics due to rotor-stator interaction, especially in high-capacity pumps (Jia 2017;Yan 2017; Cui *et al.* 2020; Zhu 2021). One component of the fluid excitation force, the hydraulic radial force, whose magnitude and direction usually vary with time, is a major cause of pump vibration. The unsteady characteristics of the hydraulic radial force have motivated a great deal of research; many scholars have quantitatively analyzed the effects of impeller-volute interaction, flow channel structure, key dimension parameters, cavitation, eccentricity, and other factors on the unsteady characteristics of the hydraulic radial force by means of experiments or numerical simulations (Adkins and Brennen 1988; Guo and Hidenobu 2003; Gonzalez *et al.* 2006; Pei *et al.* 2009; Spence and Amaral Teixeira 2009; Barrio *et al.* 2011; Khalifa *et al.* 2011; Kang and Li 2014; Hao and Tan 2018; Jia *et al.* 2019; Liu *et al.* 2020; Zhao, Y. *et al.* 2021; Meng *et al.* 2021; Song *et al.* 2021; Shi *et al.* 2022). The most common goal of optimization design for centrifugal pump units is to minimize the hydraulic radial force (Yusoff *et al.* 2016; Lu *et al.* 2015; Dai *et al.* 2015; Mou *et al.* 2016; Martynyuk and Petrov 2020; Zhao W. *et al.* 2021).

In fact, from the perspective of the pump shaft, besides the hydraulic radial force, the impeller gravity is also a radial load that cannot be ignored. Although the magnitude and direction of impeller gravity are constant, for a local position on the pump shaft, the impeller gravity will alternately generate compressive stress and tensile stress. As shown in Fig. 1, in the ideal case where the hydraulic radial force is 0, the only radial load applied by the impeller to the pump shaft is the impeller gravity. It clearly induces pump shaft deformation. For a local point A on the pump shaft, at the initial moment (θ = 0°), the maximum compressive stress $-\sigma_m$ is generated; as the shaft rotates, point A goes up to the horizontal position where the impeller gravity does not induce stress at point A, i.e., the compressive stress decreases to 0. As point A continues to rotate upward, the gravity-induced stress is transformed into tensile stress, and when point A reaches the top of the shaft, the maximum tensile stress σ_m is generated. When point A continues to rotate to the horizontal position, the tensile stress drops to 0 again. In the last quarter of the rotation, point A rotates back to the shaft bottom, and stress becomes compressive ($-\sigma_m$) again. During the whole cycle, the amplitude of the alternating stress is σ_m.

Current studies on the radial load of centrifugal pumps usually focus on the hydraulic radial force caused by the unsteady flow field, and few studies consider the influence of the impeller gravity to comprehensively analyze the effect of the total radial load on the structural vibration and fatigue.

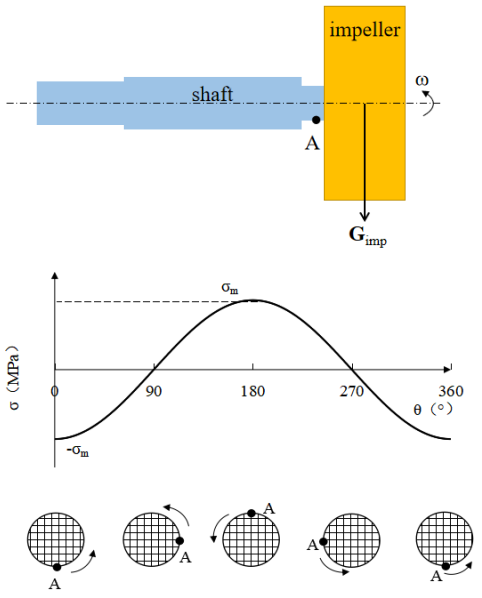

Fig. 1. Schematic diagram of stress cycle at a local position of the pump shaft caused by impeller gravity.

Considering that the scale of centrifugal pumps involved in the published literature is generally small (the outside diameter of the impeller is mostly within 250 mm), the influence of the impeller gravity is limited, which can be ignored in the study of radial load. For larger-scale dredge centrifugal pumps, the outside diameter of the impeller is usually greater than 1000 mm, and the impeller gravity should not be ignored. Fatigue fracture of large dredge pump shafts frequently occurs in engineering, but little research has been conducted on this problem. In view of the suggestion that a scientifically designed double volute can reduce the hydraulic radial force (Shi *et al.* 2013; Kim *et al.* 2016; Cui *et al.* 2018; Yuan *et al.* 2019; Zhang 2022), it would be interesting to investigate the characteristics of the corresponding total radial load and discuss the effect of the double volute in depth.

Therefore, a large centrifugal dredge pump was chosen as the research object of this study. Unsteady flow simulations were carried out for different working conditions to analyze the hydraulic radial force. Then the impeller gravity was introduced to analyze the total radial load and the alternating stress on the shaft. Finally, a double volute was applied and analyzed to show its effect on reducing radial load and stress amplitude for the pump shaft.

2. NUMERICAL MODEL

2.1 Geometry

The large centrifugal dredge pump unit in this study belonged to the DN450 series. The diameter of the suction pipe is D_1 = 450 mm, and the outside diameter of the impeller is D_2 = 960 mm. The impeller has four blades and its weight is G_{imp} = 5410 N. The rated rotational speed of the unit is n = 600 r/min. The design flow rate is Q_d = 3600 m^3/h, and the design head is H_d = 40 m. The maximum efficiency of the pump is 89.6%. The schematic diagram of the shaft is shown in Fig. 2. The minimum shaft diameter is d = 160 mm.

The three-dimensional fluid domain of the centrifugal pump is shown in Fig. 3, including the suction pipe, impeller, volute, and clearance besides the impeller. Tetrahedral unstructured mesh was used to discretize the computational domain, and the boundary layer near walls was refined with prismatic mesh. Mesh independence analysis was

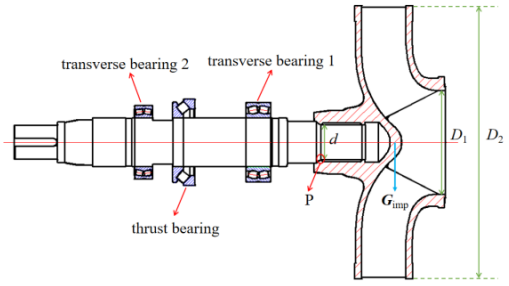

Fig. 2. Schematic diagram of the dredge pump shafting.

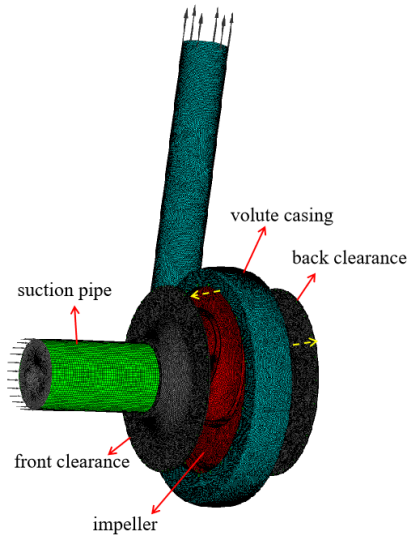

Fig. 3. Explosive view of the fluid domain.

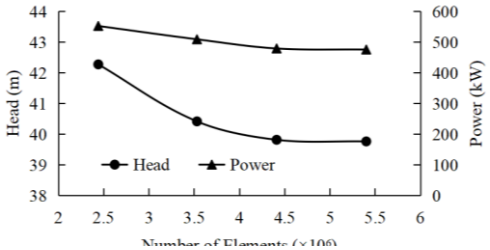

Fig. 4. Curves for mesh independence analysis.

carried out via steady simulation under the design flow rate. Figure 4 shows the variation of pump head and power with mesh quantity. The head and power both decreased with the refinement of the mesh, and the curves flattened out as the total number of mesh elements exceeded 4.4 million. Comprehensively considering calculation accuracy and simulation efficiency, the mesh of 4.4 million elements was applied to carry out the subsequent calculations.

2.2 Numerical Method

The numerical simulation of the unsteady flow field was based on the URANS method. ANSYS CFX was applied to solve the N-S equations, i.e., Eqs. (1) and (2). The curvature-corrected shear stress transfer (SST) k-ω turbulence model (Smirnov and Menter 2009) was adopted with the high-resolution scheme, i.e., Eqs. (3) and (4), which has been proved accurate in predicting flow separation in centrifugal pumps (Cao *et al.* 2015; Yuan *et al.* 2019; Cui *et al.* 2021).

$$\frac{\partial \rho}{\partial t} + \nabla \cdot (\rho \boldsymbol{u}) = 0 \tag{1}$$

$$\frac{\partial}{\partial t}(\rho \boldsymbol{u}) + \nabla \cdot (\rho \boldsymbol{u}\boldsymbol{u}) = -\nabla p + \mu \nabla \cdot \left(\nabla \boldsymbol{u} + (\nabla \boldsymbol{u})^T\right) \tag{2}$$

$$\frac{\partial \rho k}{\partial t}+\frac{\partial}{\partial x_j}\left(\rho u_j k\right)=\frac{\partial}{\partial x_j}\left[\left(\mu+\frac{\mu_t}{\sigma_k}\right)\frac{\partial k}{\partial x_j}\right] + P_k \cdot f_r-\beta^* \rho k\omega \tag{3}$$

$$\frac{\partial(\rho\omega)}{\partial t}+\frac{\partial}{\partial x_j}\left(\rho u_j \omega\right)=\frac{\partial}{\partial x_j}\left[\left(\mu+\frac{\mu_t}{\sigma_\omega}\right)\frac{\partial \omega}{\partial x_j}\right] + \alpha\frac{\rho}{\mu_t}P_k \cdot f_r-\beta\rho\omega^2+2(1-F_1)\frac{1}{\sigma_\omega \omega}\frac{\partial k}{\partial x_j}\frac{\partial \omega}{\partial x_j} \tag{4}$$

The total pressure was specified at the inlet of the suction pipe and the mass flow rate was specified at the outlet of the volute. The impeller was set as a rotating domain with a rotational speed of 600 r/min, and the other domains were static domains. The transient rotor-stator model was applied at the interfaces between impeller and other domains to deal with the data transfer. Each revolution was divided into 200 steps for calculation, i.e., the impeller rotated 1.8° in each timestep. Each calculation case lasted for 12 revolutions. The calculation step was identified as convergent when the residual was reduced to below 10^{-5}.

The hydraulic radial force $\boldsymbol{Fr}_h$ exerted by the fluid on the impeller was read from the CFD simulation result, and then the statistical analysis of the instantaneous hydraulic radial force was carried out.

3. EXPERIMENTAL VALIDATION

To verify the accuracy of the numerical method, the performance test of the pump was carried out, and the pressure pulsation near the volute tongue was monitored.

3.1 Test Rig

Figure 5 shows the hydraulic machinery test rig used in this study. Water was sucked from the underground pool, boosted by the pump, and then discharged back to the underground pool through the pipe. Two pressure transducers with measurement error less than 1% were used to measure the suction pressure and discharge pressure of the pump. An electromagnetic flowmeter with measurement error less than 1.5% was used to measure the flow rate. A torque-power meter with measurement error less than 1% was connected to the pump shaft to measure the shaft power. A high-frequency pressure pulsation sensor was mounted at point F1 to monitor the pressure near the volute tongue. Its sampling frequency was 2000 Hz, and its measurement error was less than 0.25%. The flow rate was controlled by the valve in front of the suction pipe. The pressure pulsation data was recorded for 10 s after the pressure was stabilized in each working condition. Data collection, storage, and preliminary analysis for the above transducers were conducted by a data acquisition instrument.

3.2 CFD Model Validation

The unsteady numerical simulation results of the last four revolutions were used for analysis. The time-averaged values of head and power in each working condition are shown by the solid lines in Fig. 6, and the measured results are shown by the dotted lines. The numerical simulation results were in good agreement with the measured results, and the calculation error was within 6%.

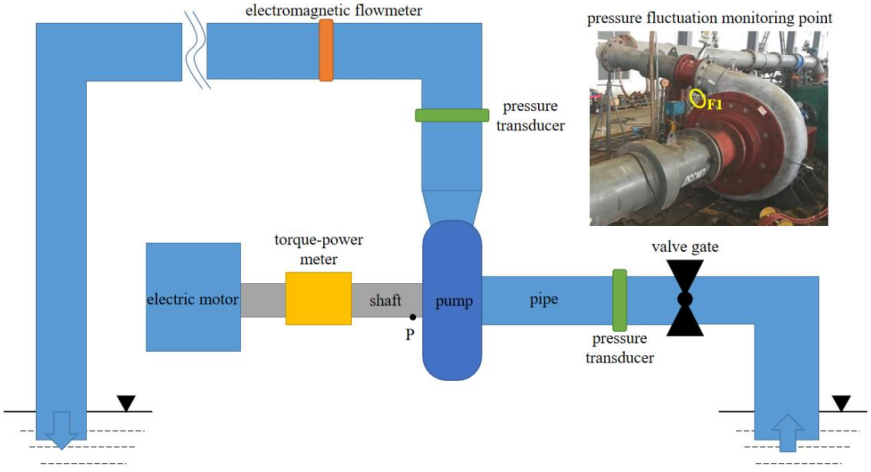

Fig. 5. Schematic diagram of hydraulic machinery test rig.

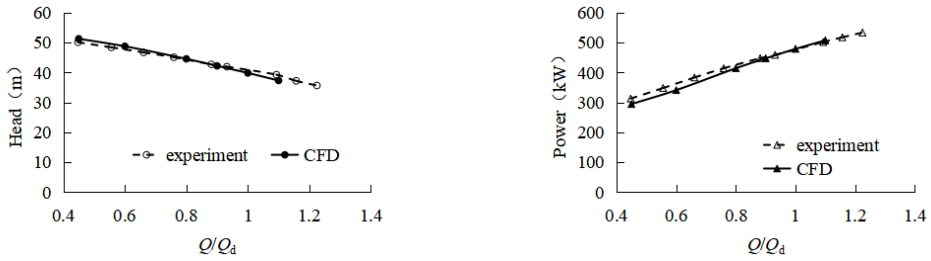

Fig. 6. Comparison of numerical and experimental performance curves.

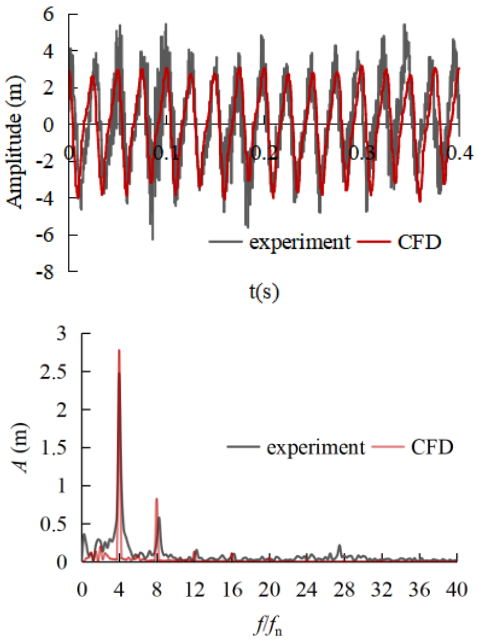

Fig. 7. Comparison of numerical and experimental pressure pulsation characteristics at point F1 in the design flow rate.

The pressure pulsation characteristics at point F1 in the design flow rate are shown in Fig. 7. The time-domain diagram (top) and spectrum diagram (bottom) show that the simulation can well capture the unsteady characteristics of the local flow field, meaning the numerical method is accurate and reliable.

4. RADIAL LOAD AND LOCAL STRESS ANALYSIS

The hydraulic radial force was calculated and analyzed for three representative conditions ($0.8Q_d$, $1.0Q_d$, and $1.1Q_d$), and the total radial loads on the shaft were compared to illustrate the influence of the impeller gravity. Then the corresponding local stress at the narrowest section of the shaft was discussed.

4.1 Radial Load

Figure 8 shows the vector diagram of the hydraulic radial force $\boldsymbol{Fr}_h$ applied to the impeller during one revolution as well as the total radial load $\boldsymbol{Fr}$ applied to the shaft. The hydraulic radial force $\boldsymbol{Fr}_h$ varied centrosymmetrically with a clear indication of four blades, and it appeared to be a relatively stable load on the shaft. The vector diagram of the total radial load $\boldsymbol{Fr}$ shifted down along the direction of gravity (-y), indicating a completely different law of direction variation of the radial load on the shaft. For the working condition of $0.8Q_d$, the direction of $\boldsymbol{Fr}$ changed within the third and fourth quadrants. For $1.0Q_d$, the direction of $\boldsymbol{Fr}$ mainly changed within the third and fourth quadrants and also within the first quadrant for a moment, whereas for $1.1Q_d$, $\boldsymbol{Fr}$ also pointed to the second quadrant for a

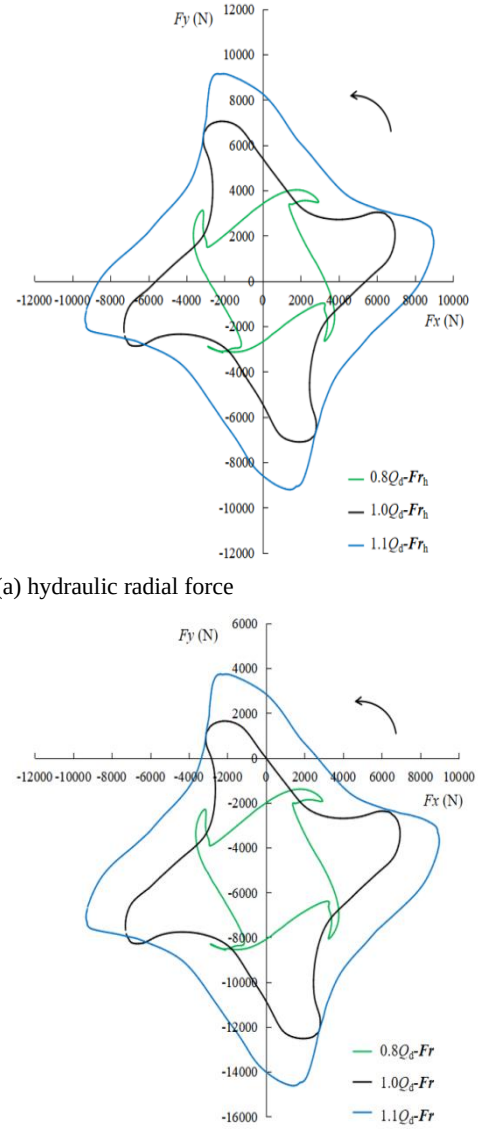

(a) hydraulic radial force

(b) total radial load

Fig. 8. Vector diagram of the radial load.

while. This kind of asymmetric change of force direction reduced the shaft stability.Fast Fourier transform analysis was performed on four-revolution data of the hydraulic radial force and total radial load to obtain the spectrum diagram shown in Fig. 9. Regarding the hydraulic radial force $\boldsymbol{Fr}_h$, the dominant frequency was four times the rotational frequency, i.e., the blade passing frequency. In the condition of $0.8Q_d$, the amplitude was smaller, whereas in the other two conditions, the amplitude was about two times larger. Regarding the total radial load $\boldsymbol{Fr}$, the dominant frequency was equal to the rotaional frequency, which was determined by the unchanged impeller gravity, and as the flow rate increased, the amplitude increased.

Therefore, the impeller gravity must be considered in the radial load analysis because it affects both the frequency and amplitude of the alternating radial load.

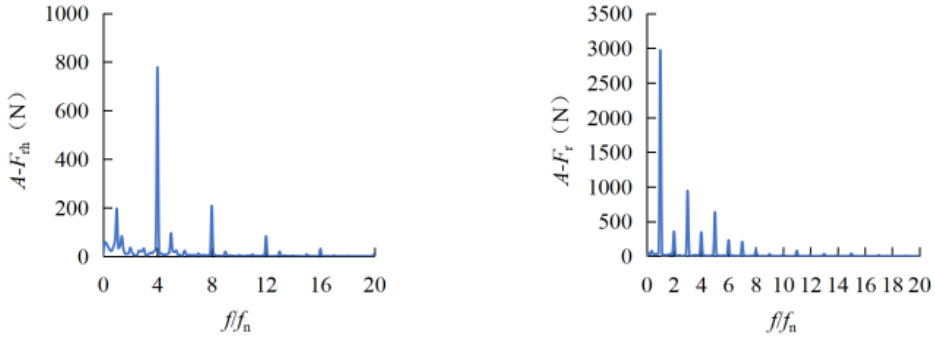

a) 0.8Q_d

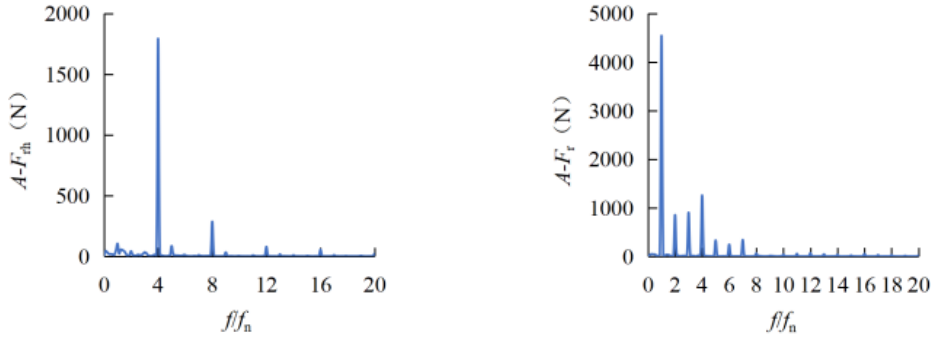

b) 1.0Q_d

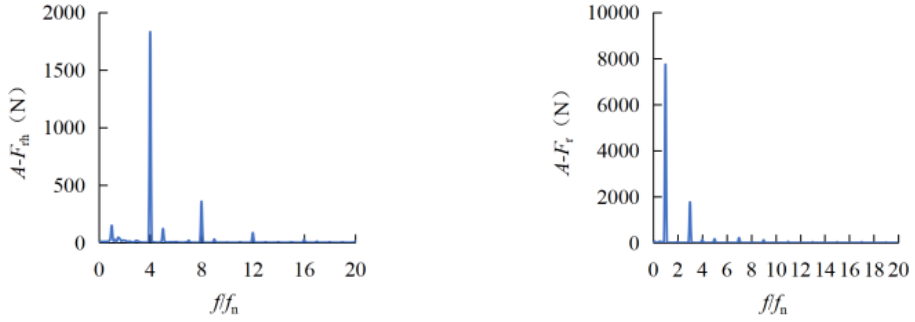

c) 1.1Q_d

Fig. 9. Spectrum diagram of the radial load.

4.2 Local Stress

Transient analysis was carried out for the shaft only with the radial load. As previously stated, the variation law of the local stress is related to the angular position of the point relative to the direction of the radial load. Hence, four points at the narrowest section of the shaft shown in Fig. 2, where fatigue fracture usually occurs, were chosen to discuss the dynamic stress. Point P_1 was located at the bottom of the shaft at the initial moment, as displayed in Fig. 10(a). The corresponding one-revolution results in the design condition are shown in Fig. 10(b)–(e), where the blue lines represent Fr_h and the black lines represent Fr. The negative values indicate compressive stress and the positive values indicate tensile stress. Axisymmetric points have completely opposite stress states. The variation frequency of the stress was similar to that of the corresponding radial load. At point P_2, the stress was almost always tensile, whereas at point P_4, the stress was almost always compressive. At points P_1 and P_3, the impeller gravity stretched the shaft, causing compressive-tensile alternating stress when the hydraulic radial force gave rise to almost pure compressive stress or tensile stress. The above stress characteristics help explain why the pump shaft usually starts to break locally.

5. RESULTS COMPARISON WITH A DOUBLE VOLUTE

Referring to previous research results, a double volute was designed to decrease the hydraulic radial force by adding a baffle to separate the downstream flow passage, as shown in Fig. 11. The baffle followed a logarithmic spiral curve whose beginning-ending connecting line passed through the center of the volute base circle and the volute tongue, and the thickness of the baffle was 10 mm.

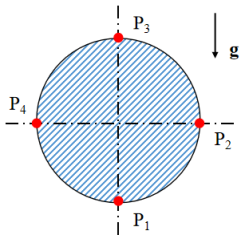

(a) positions of the four points

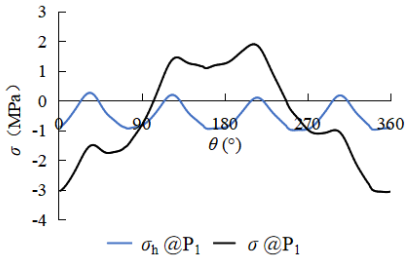

(b) stress at P_1

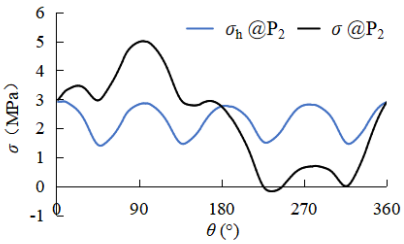

(c) stress at P_2

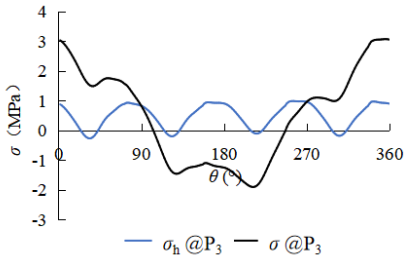

(d) stress at P_3

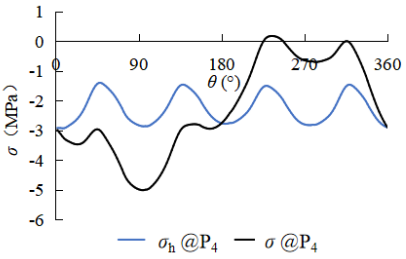

(e) stress at P_4

Fig. 10. Dynamic stress caused by the radial load in the design condition.

The performance curves of the pump corresponding to the original single volute and the double volute are compared in Fig. 12. For the three conditions simulated, the axial power was nearly unchanged, whereas the head decreased by as much as 9% with the double volute. The efficiency declined by 8% at most due to the double volute, and the maximum efficiency point shifted left to a smaller flow rate.

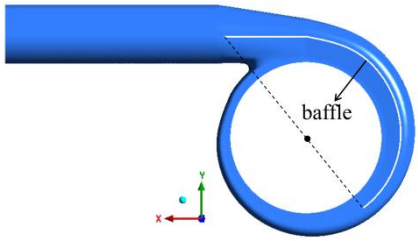

Fig. 11. Fluid domain of the double volute.

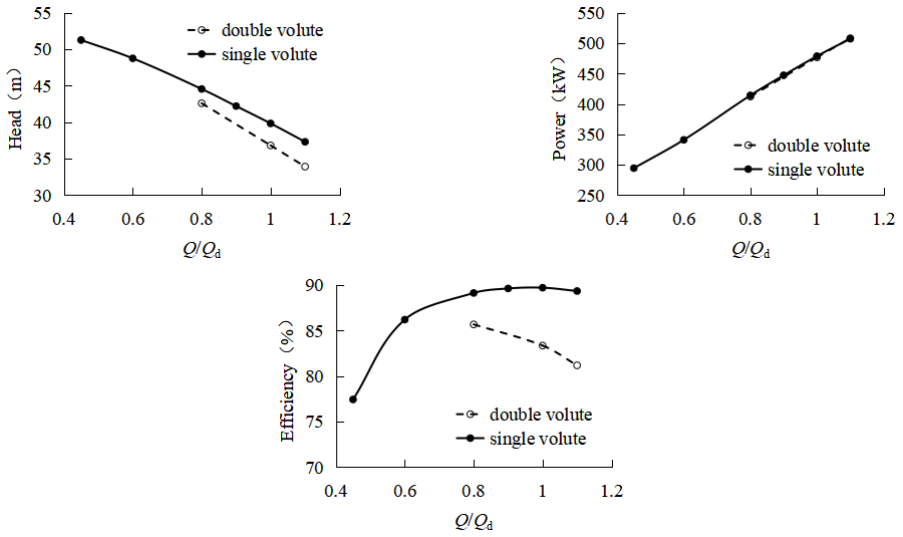

Fig. 12. Comparison of the performance curves of the pump with the single and double volutes.

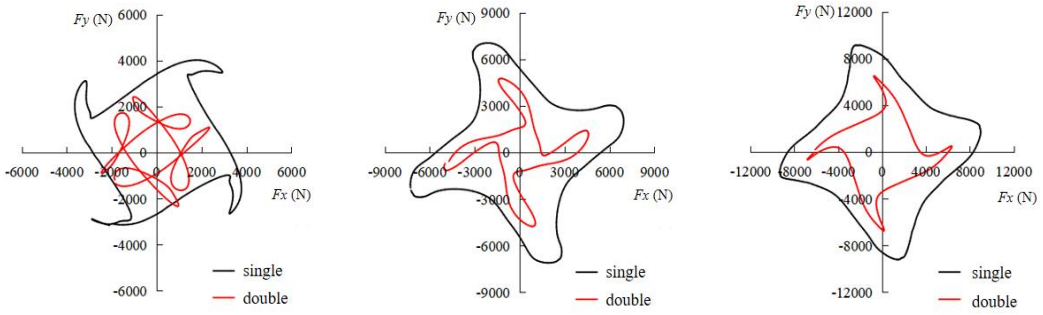

(a) $0.8Q_d$ (b) $1.0Q_d$ (c) $1.1Q_d$

Fig. 13. Comparison of the vector diagrams of the hydraulic radial force.

5.1 Radial Load

The vector diagrams of the hydraulic radial force in three typical conditions are displayed in Fig. 13, in which the black curves correspond to the single volute and the red curves correspond to the double volute. The double volute caused the hydraulic radial force to decrease, which is consistent with the conclusions of relevant literature, and it caused the shape of each vector diagram to change.

The effect of the double volute was detected by investigating the flow field. Figure 14 shows the instantaneous streamlines corresponding to the single and double volutes. The single volute matched the impeller well, so flow separation and vortexes did not appear and the pump ran at high efficiency in all three conditions. After adding the baffle to create the double volute, the upstream flow field was not disturbed, but the downstream flow rushed into two passages and generated much higher velocity in the narrow outer passage. At the end of the baffle, obvious flow separation occurred in the conditions of $1.0Q_d$ and $1.1Q_d$, resulting in higher energy consumption and lower efficiency.

Figure 15 shows the pressure coefficient on the middle section of the pump. The pressure coefficient, C_p, is defined in Eq. (5), where p_{atm} = 101,325 Pa and u_2 is the circumferential velocity at the outlet of the impeller.

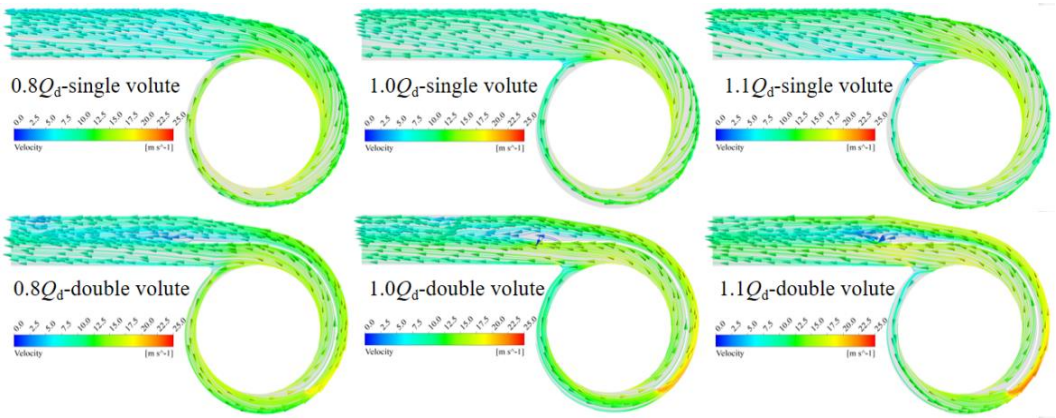

Fig. 14. Comparison of the streamlines with the single and double volutes.

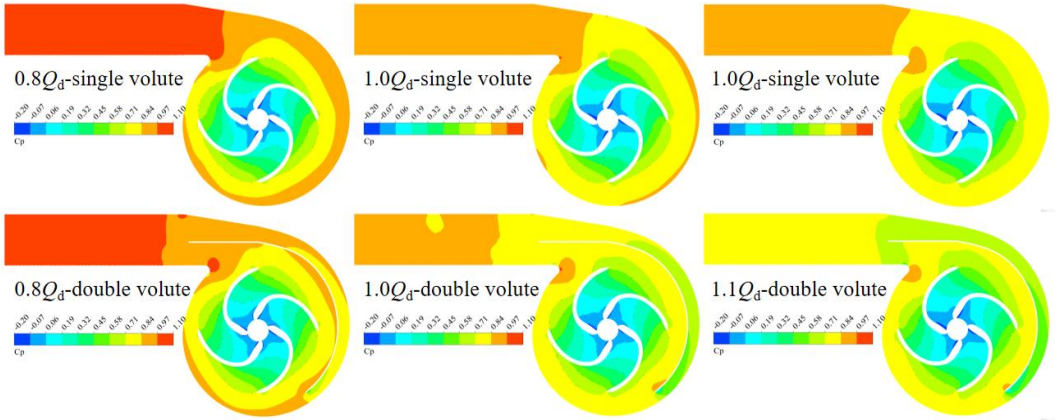

Fig. 15. Comparison of the pressure distribution in the middle section of the pump with the single and double volutes.

Table 1 Comparison of radial load (N).

	$0.8Q_d$		$1.0Q_d$		$1.1Q_d$	
	Single volute	Double volute	Single volute	Double volute	Single volute	Double volute
$Fr_{h,ave}$	3558	1789	5873	3091	7835	4836
$Fr_{h,max}$	4619	2629	7644	5154	9493	6841
$Fr_{h,min}$	2243	766	3562	1191	5589	3057
$Fr_{h,amp}$	1188	931	2041	1981	1952	1892
Fr_{ave}	5832	5488	7281	5798	8813	6604
Fr_{max}	8827	7800	12690	10203	14693	12160
Fr_{min}	1789	3146	60	1082	1927	115
Fr_{amp}	3519	2327	6315	4561	6383	6023

Comparing the single volute and double volute for each condition, the pressure distribution feature seemed similar in each condition and the main differences were around the baffle and near the outlet section. The baffle is a pressure separator. The pressure was lower outside of the baffle since the velocity was higher in this area. The pressure distribution around the impeller was more symmetrical with the double volute, and the baffle could take on part of the hydraulic pressure, so the corresponding hydraulic radial force applied on the impeller was smaller. Due to the energy dissipation caused by the baffle, the high-pressure area at the outlet section of the volute was significantly smaller than in the single volute case, and as a result, the head decreased.

$$C_p = (p - p_{atm}) / \left(\frac{1}{2} \rho u_2^2 \right) \tag{5}$$

The time-averaged total radial load (Fr_{ave}), the maximum value (Fr_{max}), the minimum value (Fr_{min}), and the fluctuation amplitude (Fr_{amp} = (Fr_{max}-Fr_{min})/2) for the three working conditions are listed in Table 1, and the data from the hydraulic radial force indicated by Fr_h are listed as well. Consistent with Fig. 13, the time-averaged hydraulic radial force $Fr_{h,ave}$ with the double volute decreased by 50% at 0.8Qd, 47% at 1.0Qd, and 38% at 1.1Qd. However, the total radial load Fr_{ave} with the double volute decreased by just 6%, 20%, and 25%, and its change rule with the flow rate was opposite to that of the hydraulic radial force.

Regarding the fluctuation characteristics, the amplitude of the hydraulic radial force $Fr_{h,amp}$ was reduced by 22%, 3%, and 3% at $0.8Q_d$, $1.0Q_d$, and $1.1Q_d$, respectively, under the influence of the double volute. The total radial load Fr_{amp} was reduced by 34%, 28%, and 6% for the three conditions. The minimum values of Fr_{ave} and Fr_{amp} both occurred in the condition of $0.8Q_d$, whose efficiency was the highest among the three conditions.

To sum up, a double volute can reduce the hydraulic radial force applied to the impeller by nearly half, but it has a limited effect on reducing the fluctuation amplitude. Considering the constant impeller gravity, the reduction of the total radial load applied on the shaft is less significant, whereas the reduction of fluctuation amplitude is prominent, especially in part-load conditions, which will decrease shaft vibration.

5.2 Local Stress

Transient analysis was also conducted for the shaft with the decreased radial load to check the effect of the double volute on reducing fatigue risk. In Table 2, the key data of the local stress at point P1 with the two volutes are compared. Under the influence of the double volute, the time-averaged compressive stress (σ_{ave}) decreased in the condition of $0.8Q_d$, and the time-averaged tensile stress slightly increased in the conditions of $1.0Q_d$ and $1.1Q_d$.

Table 2 Stress data at point P1 (MPa)

	$0.8Q_d$		$1.0Q_d$		$1.1Q_d$	
	Single volute	Double volute	Single volute	Double volute	Single volute	Double volute
σ_{ave}	−1.31	−0.44	0	0.14	0.02	0.66
σ_{max}	0.78	1.61	3.14	2.27	2.52	2.94
σ_{min}	−3.51	−2.66	−5.09	−2.38	−2.73	−2.1
$\Delta\sigma$	2.14	2.14	4.11	2.32	2.62	2.52

When the structure was changed from the single volute to the double volute, the maximum and minimum values of the stress shifted in the positive direction, i.e., the compressive stress decreased and the tensile stress increased, in the conditions of $0.8Q_d$ and $1.1Q_d$. The maximum and minimum stress varied at the same level, so the corresponding amplitude $\Delta\sigma$ remained nearly unchanged (within 4%). In the condition of $1.0Q_d$, the minimum compressive stress (σ_{min}) and the maximum tensile stress (σ_{max}) both decreased, and $\Delta\sigma$ prominently decreased by about 44%. With the double volute, $\Delta\sigma$ became similar among the three conditions. Since $\Delta\sigma$ is a key parameter related to the fatigue damage, the application of the double volute will help prolong the fatigue life of the shaft which usually operates in the design condition.

The variation laws of the local stress and the radial load are different, and the impeller gravity plays a key role in each variation law. The hydraulic optimization of a centrifugal pump should consider not only the hydraulic radial force but also the dynamic stress of the shaft. A double volute is not always the best choice for engineering applications, so designers should balance the energy performance and vibration characteristics of the pump unit based on the intended application.

6. CONCLUSION

In this study, the hydraulic radial force on the impeller and the total radial load were calculated via unsteady numerical simulations for a large centrifugal dredge pump. The flow field with a double volute was also analyzed and compared to the flow field with the single volute. Stress analysis was carried out to illustrate the influence of the impeller gravity and the double volute. The conclusions are as follows:

(1) The total radial load on the pump shaft includes the hydraulic radial force and the gravity of the impeller. The impeller gravity is large enough to determine the fluctuation frequency of the radial load on the shaft and increase its time-averaged value. Therefore, the impeller gravity should not be ignored in the analysis of radial load for large-scale centrifugal pumps.

(2) The characteristics—especially the tensile and compressive states— of the stress induced by the radial load, which fluctuate in an asymmetric cycle, are different at different circumferential locations on the same section of the shaft, which will result in different fatigue risks. This explains why fatigue cracks first appear in certain locations even if the shaft is well manufactured. The direction of the radial load with respect to the stress location under study plays a decisive role in this phenomenon.

(3) The application of a double volute decreases the time-averaged value and fluctuation amplitude of both the hydraulic radial force and the total radial load. The double volute affects the local stress and the radial load to different degrees. The amplitude reduction of shaft stress in the design condition will prolong the expected fatigue life. However, the double volute decreases the pump head and efficiency, so whether a double volute is worth using in practical application depends on the specific situation.

ACKNOWLEDGEMENTS

This work was supported by China Communications Construction Company Limited (grant number 2019-ZJKJ-PTJS06). We thank LetPub (www.letpub.com) for its linguistic assistance during the preparation of this manuscript.

REFERENCES

Adkins, D. and C. E. Brennen (1988). Analysis of hydrodynamic radial forces on centrifugal pump impellers. *ASME Journal of Fluids Engineering* 110(1), 20-28.

Barrio, R., J. Fernández, E. Blanco and J. Parrondo (2011). Estimation of radial load in centrifugal pumps using computational fluid dynamics. *European Journal Mechanics B/Fluids* 30(3), 316-324.

Brennen, C. E. (2011). *Hydrodynamics of Pumps.* Cambridge University Press, New York, USA.

Cao, L., Y. Zhang, Z. Wang, Y. Xiao and R. Liu (2015). Effect of axial clearance on the efficiency of a shrouded centrifugal pump. *Journal of Fluids Engineering* 137(7), 071101.

Cui, B., J. Li, C. Zhang and Y. Zhang (2020). Analysis of radial force and vibration energy in a centrifugal pump. *Mathematical Problems in Engineering* 2020, 1-12.

Cui, B., X. Li, K. Rao, X. Jia and X. Nie (2018). Analysis of unsteady radial forces of multistage centrifugal pump with double volute. *Engineering Computations* 35(3), 1500-1511.

Dai, C., Dai, F. Kong, L. Dong, H. Zhang and Z. Feng (2015). Effect of blade wrap angle on the radial force of centrifugal pump as turbine. *Journal of Vibration and Shock* 34(18), 69-72+99.

Gonzalez, J., J. Parrondo, C. Santolaria and E. Blanco (2006). Steady and unsteady radial forces for a centrifugal pump with impeller to tongue gap variation. *ASME Journal of Fluids Engineering* 128(3), 454-462.

Guo, S. and O. Hidenobu (2003). An experimental study on the fluid forces induced by rotor-stator interaction in a centrifugal pump. *International Journal of Rotating Machinery* 9(2), 135-144.

Hao, Y. and L. Tan (2018). Symmetrical and unsymmetrical tip clearances on cavitation performance and radial force of a mixed flow pump as turbine at pump mode. *Renewable Energy* 127, 368-376.

Jia, Q. (2017). *Investigation on Unstable Flow and Vibriation Characteristics of a Centrifugal Pump*. Ph. D. thesis, Zhejiang University, Hanzhou, China. (In Chinese)

Jia, X., Jia, S. Yuan, Z. Zhu and B. Cui (2019). Numerical study on instantaneous radial force of a centrifugal pump for different working conditions. *Engineering Computations* 37(2), 458-480.

Kang, C. and Y. Li (2014). The effect of twin volutes on the flow and radial hydraulic force production in a submersible centrifugal pump. *Proceedings of the Institution of Mechanical Enginners Part A - Journal of Power and Energy* 229(a2), 221-237.

Khalifa, A. E., A. M. Al-Qutub and R. Ben-Mansour (2011). Study of pressure fluctuations and induced vibration at blade-passing frequencies of a double volute pump. *Arabian Journal for Science and Engineering* 36(7), 1333-1345.

Kim, K., H. Shim, A. Afzal and H. Jeong (2016). Three-objective optimization of a centrifugal pump with double volute to minimize radial thrust at off-design conditions. *Proceedings of the Institution of Mechanical Engineers* 230(6), 598-615.

Liu, Y., J. Gong, K. An and L. Wang (2020). Cavitation Characteristics and Hydrodynamic Radial Forces of a Reversible Pump–Turbine at Pump Mode. *Journal of Energy Engineering*, 146(6), 04020066.

Lu, G., Z. Zuo, S. Liu, Y. Fan and Y. Wu (2015). Numerical analysis of the influence of casing ’s shape on the radial force of a centrifugal pump. *Journal of Engineering Thermophysics* 36(4), 770-774.

Lu, Z., N. Li, R. Tso, Z. Yao, E. Liu and R. Xiao (2022), Influence of eccentric impeller on pressure pulsation of large-scale vaned-voluted centrifugal pump. *Proceedings of the Institution of Mechanical Enginners Part A - Journal of Power and Energy*.

Martynyuk O. and A. Petrov (2020). Experience in calculating the annular discharge of a centrifugal pump based on the hydrodynamic modeling method. *IOP Conference Series: Materials Science and Engineering* 963, 012023.

Meng, D., T. Jiang, H. Deng and G. Hou (2021). Numerical Simulation Research on Radial Force of Centrifugal Pump with Guide Vanes. *Shock and Vibration*, 2021, 6638123.

Mou, J., Mou, J. Liu, Y. Gu, D. Dai, S. Zheng and Y. Ma (2016). Effect of different tongues on radial hydraulic force characteristics and internal flow field of a centrifugal pump. *Journal of Vibration and Shock* 35(11), 116-122.

Pei, J., S. Yuan, J. Yuan and L. Yin (2009). Numerical analysis on asymmetrical distribution of flow field and radial force for a centrifugal pump. In *Proceedings of the 2009 International Conference on Energy and Environment Technology*, Washington, USA.

Shi, H., J. Mou, S. Zhen, J. Gan, L. Lin and W. Fan (2013). Effect of different baffle length of double volute pump on radial force balance. *Acta Agriculturae Zhejiangensis* 25(6), 1378-1382. (In Chinese)

Shi, W., C. Chen, L. Tan and Z. Shi (2022). Experimental study on the single blade centrifugal pump radial force. *Journal of Vibration and Shock* 41(2), 185-192.

Smirnov, P. E. and F. R. Menter (2009). Sensitization of the SST turbulence model to rotation and curvature by applying the spalart-shur correction term. *Journal of Turbomachinery* 131(4), 041010.

Song, Y., H. Fan and Z. Huang (2021). Study on radial force characteristics of double-suction centrifugal pumps with different impeller arrangements under cavitation condition. *Proceedings of the Institution of Mechanical Engineers, Part A: Journal of Power and Energy* 235(3), 421-431.

Spence, R. and J. Amaral Teixeira (2009). A CFD parametric study of geometrical variations on the pressure pulsations and performance characteristics of a centrifugal pump. *Computers & Fluids* 38(6), 1243-1257.

Tan, M., Y. Lu, X Wu, H. Liu and X Tian (2021). Investigation on performance of a centrifugal pump with multi-malfunction. *Journal of Low Frequency Noise Vibration and Active Control* 40(2), 740-752.

Yan, P. (2017). *Research on Unsteady Characteristics and Flow Induced Vibration of Large Flow Rate Pumps*. Ph. D. thesis, Zhejiang university, Hanzhou, China. (In Chinese)

Yuan, Y., S. Yuan and L. Tang (2019). Numerical investigation on the mechanism of double-volute balancing radial hydraulic force on the centrifugal pump. *Proces*ses 7(10), 689.

Yusoff, M. D., M. H. Lim, M. R. Yahaya and J. Azman (2016). Exit geometry modifications of double volute centrifugal pump for vane passing frequency vibration resolution: a case study. *Advanced Engineering Forum* 16, 82-90.

Zhang, H. (2022). *Research on the Influence of the Double Tongue Volute Structure on the Plastic Centrifugal Pump Performance*. M.D. thesis, Anhui Polytechnic University, Wuhu, China. (In Chinese)

Zhao, W., S. Chen, Q. Zhao, D. Ma, Y. Liang and H. Peng (2021). Effect of blade arrangement on radial force of double suction centrifugal pump. *Journal of Drainage and Irrigation*

Machinery Engineering 39(4), 331-337. (In Chinese)

Zhao, Y., X. Wang and R. Zhu (2021). Effect of eccentricity on radial force and cavitation characteristics in the reactor coolant pump. *Thermal Science* 25(5A), 3269-3279.

Zhu, A. (2021). *Numerical Simulation and Experimental Study on Radial Force of Centrifugal Pump*. M.D. thesis, Shenyang University of Technology, Shenyang, China. (in Chinese)